IET Journals
The Institution of Engineering and Technology

Optimal configuration of hybrid Hydrogen-to-Power system for power systems with high penetration of renewable energy

ISSN 1751-8644
doi: 0000000000
www.ietdl.org

Hongzhen Wang[1], *Boyu Qin*[1], *Tao Ding*[1], *Fan Li*[2]

[1] *School of Electrical Engineering, Xi'an Jiaotong University, Xi'an 710049, China*
[2] *State Grid Economic and Technological Research Institute Company, Ltd., Beijing 102209, China*
* *E-mail: qinboyu@xjtu.edu.cn*

Abstract: Hydrogen energy plays an important role in improving the operation efficiency and reliability of power systems with high renewable energy penetration. Hydrogen to power (HtP) system is the key link of hydrogen applications. However, the single HtP equipment is limited in power output range and efficiency. Hybrid HtP system is an important scheme to realize the performance complementary. However, the hybrid HtP system is coupled with hydrogen system and power system. The characteristics of each subsystem and coupling characteristics are complex. In addition, the multiple support potential of hybrid HtP system for power system needs to be fully explored. In this paper, firstly, a power system including traditional units, high penetration renewable energy generation and hybrid HtP system is established. Secondly, a bi-level hybrid HtP system optimal configuration model including planning and operation is constructed. Then, a bi-level optimal configuration method based on improved PSO algorithm is proposed. Finally, the optimization model and its solution method are applied to IEEE one area RTS-96. The discussions based on the optimization results show that the hybrid HtP system has significant contributions in optimizing the output cost of traditional units, improving the utilization of renewable energy, and reducing load shedding losses.

1 Introduction

In the context of global climate change and energy security, hydrogen energy has gained increasing prominence as a means to advance the utilization of renewable energy sources [1], enable long-term and large-scale storage of electric energy [2, 3], enhance the flexible regulation capabilities of power systems [4, 5], and facilitate the interconnection of various energy networks [6, 7]. The hydrogen-to-power (HtP) system serves as the pivotal link between the power system and the hydrogen system, playing a significant role in realizing the end-user functionalities of the energy system. The planning and operation of HtP system profoundly impact the overall efficiency of the energy utilization pathway [8–10]. Consequently, investigating the configuration methodology for coupling the HtP system with the power system and hydrogen system holds substantial significance.

According to different power generation equipment, HtP system can generally be divided into hydrogen fuel cell (HFC), hydrogen fuel gas turbine (HFGT) and hydrogen internal combustion engine (HICE) [11].HFC directly converts the chemical energy of fuel into electrical energy through non combustion [12]. Compared with conventional power generation technology, its power generation efficiency is not limited by Carnot cycle, and the power generation efficiency can reach 60%-70% [13]. It also has the advantages of zero emission and no noise during operation. At present, the HFC under research and development mainly include proton exchange membrane fuel cell, oxide fuel cell, alkaline fuel cell, phosphoric acid fuel cell and high temperature molten carbonate fuel cell [14]. However, HFC have high requirements for hydrogen purity, difficult to expand power, and high power generation costs, which limit their application in high-power scenarios [15]. The HFGT efficiently converts fuel energy into mechanical energy through the combustion of hydrogen, subsequently transforming it into electrical energy. HFGT typically exhibits greater power output compared to HFC, albeit at a lower level of efficiency [16]. Moreover, the interchangeability of HFGT and natural gas turbine is good, and natural gas turbine can realize hydrogen combustion through burner transformation [17]. Indeed, the development of HFGT is rooted in the existing hydrogen-blended combustion technology of gas turbines, offering unmistakable advantages [18]. In 2022, the incorporation of 30% hydrogen into a 54 MW gas turbine in Jingmen, China, resulted in a reduction of over 18,000 tons of CO_2 emissions annually [19]. HICE shares similarities with HFGT, while it significantly lags behind in power output and has more NO_x emissions[20].

The configuration of the HtP system often depends on various application scenarios, with a primary focus on the renewable energy power systems. In [21], a wind-solar-battery-fuel cell system is established to optimize the average annual cost and the loss of power supply probability. In [22], an algorithm is proposed to obtain the optimal configuration of photovoltaic, fuel cell, and biomass-based hybrid energy system. In [23], a novel deviation satisfaction strategy is proposed to solve the configuration optimization of the natural gas-wind-photovoltaic-hydrogen integrated energy system. However, The above researches primarily focus on systems employing a single type of HtP equipment, such as HFC or HFGT. This approach faces challenges in meeting the power demands of power systems with a wide range power range. In reality, HFC and HFGT exhibit complementary power output characteristics [24]. The construction of a hybrid HtP system incorporating both HFC and HFGT would significantly enhance the performance and dispatching flexibility of the HtP system. In [25], a solid oxide fuel cell/gas turbine hybrid system is constructed and operates with low wind curtailment rate and high renewable penetration level. In [26], a solid oxide fuel cell and gas turbine based co-generation system is proposed to analyze the co-generation system performance from the perspective of thermodynamic and economic costs. Reference [27] evaluates the performance of particle swarm optimization (PSO) and genetic algorithm (GA) for optimizing integrated solid oxide fuel cell-gas turbine system. Nevertheless, the researches discussed above do not fully exploit the potential support offered by a hybrid HtP system within the energy system. This untapped potential includes improving the level of renewable energy accommodation, reducing the

output cost of traditional units, and enhancing the reliability of power system. It is imperative to fully considered in the optimal configuration of hybrid HtP system to improve the comprehensive benefits of the system.

In this paper, we develop an optimal configuration model of hybrid HtP system considering the stage of planning and operation. First, the traditional unit operation model, renewable energy generation model, hybrid HtP system operation model and power grid operation model are constructed. Second, the optimal configuration model of hybrid HtP system is established considering the renewable energy generation, traditional unit output cost and load shedding. Third, a bi-level optimal configuration method based on improved PSO algorithm is proposed to solve the two stage optimization. The main contributions of the paper are as follows:

(1)The operation model of hybrid HtP system is formulated. The model achieves the conversion of hydrogen electrical energy at various power scales, , while also facilitating energy interactions between the power system and the hydrogen system.
(2)The optimal configuration model of hybrid HtP system is established and solved as Mixed-Integer Linear Programming (MILP). Renewable energy utilization, traditional unit output cost and load shedding are have been considered in the optimization objective.
(3)A bi-level optimization configuration method is proposed to solve planning and operational optimization problems, and an improved PSO algorithm is introduced to improve the solution accuracy.

The rest of this paper is organized as follows. Section 2 describes the operation model of traditional unit, renewable generation, hybrid HtP system and power grid. Section 3 presents the optimal configuration model of hybrid HtP system. Section 4 clarifies the bi-level optimal configuration method for solving the optimal configuration model. Section 5 conducts a case study based on the modified IEEE RTS-96. Finally, Section 6 describes the conclusion of this paper.

2 Power system operation model considering hybrid HtP system

High penetration renewable energy power system is the basis of the construction and operation of hybrid HtP system. In this section, the power system will be divided into different components to model. These subsystems include traditional units, renewable energy power generation, hybrid HtP system and power grid. The chematic diagram of the system is shown in Fig. 1. The modeling scope $\mathbf{T}$ is divided into equal time intervals with a length of Δt = 1h and indexed by t.

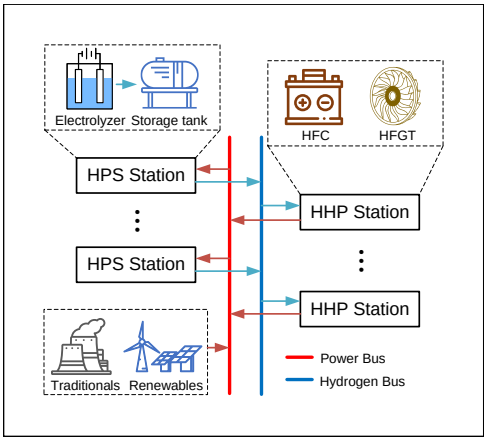

Fig. 1: The schematic diagram of power system with hybrid HtP system

2.1 Traditional unit operation model

The traditional unit has strong power grid stability support ability and withstand disturbance ability, which can maintain sufficient moment of inertia and strong frequency regulation ability of the system. Therefore, even in the high penetration renewable energy power system, the traditional unit is indispensable. The traditional unit operation model is constructed based on the unit commitment problem [28]. Considering the output constraints of the unit, the upper and lower power generation limits are as follows:

$$P_g^{Gmin} u_{g,t} \leq P_{g,t}^G \leq P_g^{Gmax} u_{g,t} - P_{g,t}^R, \forall g \in \mathbf{G}, t \in \mathbf{T} \quad (1)$$

where $\mathbf{G}$ is the set of generators in the system and is indexed by g; P_g^{Gmin} and P_g^{Gmax} are the minimal and maximal output of the g-th generator; $u_{g,t}$ is the commitment status for the g-th generator in the t-th time period and is a binary variable. $P_{g,t}^G$ is the output of generator of the g-th generator in the t-th time period. $P_{g,t}^R$ is the spinning reserve from the g-th generator in the t-th time period.

The spinning reserve needs to fulfill the additional active output required by load fluctuation, load forecast deviation and unexpected shutdown. The spinning reserve requirements of generator are as follow:

$$0 \leq P_{g,t}^R \leq R_g^{10} u_{g,t}, \forall g \in \mathbf{G}, t \in \mathbf{T} \quad (2)$$

$$P_{g,t}^G + P_{g,t}^R \leq \sum_{m \in \mathbf{G}} P_{m,t}^G u_{m,t}, \forall g \in \mathbf{G}, t \in \mathbf{T} \quad (3)$$

where R_g^{10} is outage ramping limit in 10 minutes for g-th generator.

The output that the generator can increase and decrease in unit time is limited. The variation depends on ramp rate limits.

$$-R_g \leq P_{g,t}^G - P_{g,t-1}^G \leq R_g, \forall g \in \mathbf{G}, t \in \mathbf{T} \quad (4)$$

where R_g is the maximum ramp rate of g-th generator.

The minimum up-time/down-time refers to the hours that the unit must shutdown/startup at least once it is in the shutdown/startup state. Generally, the larger the capacity of the unit, the longer the minimum up-time/down-time.

$$u_{g,t} - u_{g,t-1} \leq v_{g,t}, \forall g \in \mathbf{G}, t \in \mathbf{T} \quad (5)$$

where $v_{g,t}$ is a binary variable to indicate the startup status of the g-th generator in the t-th time period.

2.2 Renewable energy generation model

Unlike traditional units, renewable energy output is intermittent and volatile. These characteristics are reflected in renewable energy generation, that is, some renewable energy power will not be accepted by the power grid. Taking wind power as an example, the wind power that cannot be accommodated is called wind curtailment, which can be expressed as follows.

$$0 \leq P_{w,t}^{WC} \leq P_{w,t}^W, \forall w \in \mathbf{W}, t \in \mathbf{T} \quad (6)$$

where $\mathbf{W}$ is the set of wind farms in the system and is indexed by w; $P_{w,t}^{WC}$ is the wind curtailment of the w-th wind farm in the t-th time period; $P_{w,t}^W$ is the total wind power output of the w-th wind farm in the t-th time period.

In order to quantify the level of renewable energy in the power system, renewable energy penetration is introduced as follows, which is defined as the ratio of renewable energy generation to the total power consumption of the system.

$$REP = \frac{\sum_{w \in \mathbf{W}, t \in \mathbf{T}} P_{w,t}^W}{\sum_{n \in \mathbf{N}, t \in \mathbf{T}} P_{n,t}^L} \quad (7)$$

where $\mathbf{N}$ is the set of power nodes in the system and is indexed by n; $P_{n,t}^L$ is the load at node n in the t-th time period.

2.3 Hybrid HtP system operation model

In the hybrid HtP system, HFC and HFGT participate as two kinds of HtP conversion equipment. The operation of the hybrid HtP system is not only determined by the inherent characteristics of the HtP equipment, but also affected by the upstream hydrogen supply system. In the power system with high penetration of renewable energy, the hydrogen supply system is mainly composed of electrolytic hydrogen production system and hydrogen storage system. Hydrogen production and hydrogen storage are located in the same place, and these two processes are completed by building hydrogen production and storage (HPS) stations. The constraints of hydrogen production and storage are as follows:

$$0 \leq E_{e,t} \leq E_e^{rated}, \forall e \in \mathbf{E}, t \in \mathbf{T} \tag{8}$$

$$0 \leq P_{e,t}^{E} \leq P_e^{Erated}, \forall e \in \mathbf{E}, t \in \mathbf{T} \tag{9}$$

where $\mathbf{E}$ is the set of HPS stations in the system and is indexed by e; $E_{e,t}$ is the capacity of hydrogen stored at the e-th HPS station in the t-th time period; E_e^{rated} is the rated hydrogen storage capacity of the e-th HPS station; $P_{e,t}^{E}$ is the input power of electrolytic cell at the e-th HPS station in the t-th time period; P_e^{Erated} is the rated input power of electrolytic cell at the e-th HPS station.

Similarly, hybrid hydrogen to power (HHP) stations are set in the power grid for the centralized management of HtP system. It is worth noting that HFC and HFGT are not necessarily configured or operated simultaneously in one HHP station. In order to clarify the operation interaction between different HPS stations and HHP stations, the input hydrogen power of HFC and HFGT is defined more carefully considered the differences of different HPS stations. The operation limits of HFC and HFGT are as follows:

$$0 \leq \sum_{e \in \mathbf{E}} P_{f,e,t}^{F} \leq P_f^{Frated}, \forall f \in \mathbf{F}, t \in \mathbf{T} \tag{10}$$

$$0 \leq \sum_{e \in \mathbf{E}} P_{s,e,t}^{S} \leq P_s^{Srated}, \forall s \in \mathbf{S}, t \in \mathbf{T} \tag{11}$$

where $\mathbf{F}$ is the set of HFCs in the system and is indexed by f; $P_{f,e,t}^{F}$ is the input hydrogen power of the f-th HFC from the e-th HPS station in the t-th time period; P_f^{Frated} is the rated input hydrogen power of the f-th HFC; $\mathbf{S}$ is the set of HFGTs in the system and is indexed by s; $P_{s,e,t}^{S}$ is the input hydrogen power of the s-th HFGT from the e-th HPS station in the t-th time period; P_s^{Srated} is the rated input hydrogen power of the s-th HFGT.

Between HHP station and HPS station, a hydrogen transmission pipeline is required for the interaction of hydrogen energy in the whole system. In practical engineering, this task is usually done by the mature natural gas pipeline, and is realized by blending hydrogen with natural gas [29]. At the transmission terminal, this hydrogen blended natural gas can be directly used by HFGT, or pure hydrogen can be obtained by membrane separation for HFC [30, 31]. However, limited by pipeline specifications and hydrogen blending ratio, the transmission capacity of hydrogen doped natural gas pipeline needs to be limited. The constraint can be constructed as follows:

$$\sum_{f \in \mathbf{F}(n)} P_{f,e,t}^{F} + \sum_{s \in \mathbf{S}(n)} P_{s,e,t}^{S} \leq P^{Tmax} , \forall n \in \mathbf{N}, e \in \mathbf{E}, t \in \mathbf{T} \tag{12}$$

where $\mathbf{F}(n)$ and $\mathbf{S}(n)$ represent the sets of HFCs and HFGTs at node n; P^{Tmax} is the maximum transmission capacity of hydrogen blended natural gas pipeline.

Based on the HPS station model, HHP station model and hydrogen transmission model, the hydrogen balance model is constructed as follows :

$$\begin{aligned} E_{e,t} = E_{e,t-1} + \eta_e P_{e,t}^{E} - \sum_{f \in \mathbf{F}} P_{f,e,t}^{F}/\eta_f \\ - \sum_{s \in \mathbf{S}} P_{s,e,t}^{S}/\eta_s, \forall e \in \mathbf{E}, t \in \mathbf{T} \end{aligned} \tag{13}$$

where η_e is the efficiency of electrolytic hydrogen production; η_f and η_s are the generation efficiency of HFC and HFGT.

2.4 Power grid operation model

The subsystem model of power system constructed above does not involve reactive power, nor does it consider the influence of voltage distribution. Therefore, in the power grid model, the DC power flow model can be used to linearize the power grid model. The active power flowing on the branch is given by

$$P_{b,t} = \theta_{b,t}/x_b, \forall b \in \mathbf{B}, t \in \mathbf{T} \tag{14}$$

where $\mathbf{B}$ is the set of branches in the system and is indexed by b; $P_{b,t}$ is the active power flowing on the branch b in the t-th time period; $\theta_{b,t}$ and x_b are the phase difference of voltages and branch impedance of the branch b, respectively. The phase difference of voltages can be further defined as follows:

$$\theta_{b,t} = \delta_{i,t} - \delta_{j,t}, \forall b \in \mathbf{B}, t \in \mathbf{T} \tag{15}$$

$$-\pi/2 \leq \delta_{n,t} \leq \pi/2, \forall n \in \mathbf{N} \setminus n_s, t \in \mathbf{T} \tag{16}$$

where i and j are the node numbers at both ends of branch b; $\delta_{n,t}$ is the voltage phase at node n in the t-th time period. n_s indicates slack node and its voltage phase is always 0.

In order to ensure the safe operation of the transmission line, the flowing power of each branch is limited as follows:

$$-P_b^{max} \leq P_{b,t} \leq P_b^{max}, \forall b \in \mathbf{B}, t \in \mathbf{T} \tag{17}$$

where P_b^{max} is the maximum transmission power of branch b.

Based on the traditional unit operation model, renewable energy generation model, hybrid HtP system operation model and power grid operation model established above, the following real-time node power balance equation is constructed:

$$\begin{aligned} \sum_{g \in \mathbf{G}(n)} P_{g,t}^{G} + \sum_{b \in \mathbf{B}(n)} P_{b,t} + \sum_{w \in \mathbf{W}(n)} \left(P_{w,t}^{W} - P_{w,t}^{WC} \right) \\ + \sum_{f \in \mathbf{F}(n)} \sum_{e \in \mathbf{E}} P_{f,e,t}^{F} + \sum_{s \in \mathbf{S}(n)} \sum_{e \in \mathbf{E}} P_{s,e,t}^{S} \\ = \left(P_{n,t}^{L} - P_{n,t}^{LS} \right) + \sum_{e \in \mathbf{E}(n)} P_{e,t}^{E}, \forall n \in \mathbf{N}, t \in \mathbf{T} \end{aligned} \tag{18}$$

where $P_{n,t}^{LS}$ is the load shedding at node n in the t-th time period.

3 Optimal configuration of hybrid HtP system

The optimal configuration of hybrid HtP system aims to obtain the optimal location and capacity of HFC and HFGT in the power system, which involves two stages of planning and operation. Considering the feasibility and solution speed of the optimization, the planning and operation will be divided into two stages. The optimal configuration scheme will be obtained through the iteration between the two stages.

3.1 Cost of operation and planning

The optimization objective of operation is to minimize the operation cost, which is composed of three parts: traditional unit generation cost, wind curtailment penalty cost and load shedding penalty cost.

The generation cost of the traditional unit consists of three parts: operational cost, no-load cost and startup cost. The wind curtailment penalty cost and load shedding penalty cost are linear with power.

$$C_{g,t}^{gen} = c_g P_{g,t}^G + c_g^N u_{g,t} + c_g^S v_{g,t}, \forall g \in \mathbf{G}, t \in \mathbf{T} \quad (19)$$

$$C_{w,t}^{wcur} = c_w P_{w,t}^{WC}, \forall w \in \mathbf{W}, t \in \mathbf{T} \quad (20)$$

$$C_{n,t}^{shed} = c_l P_{n,t}^{LS}, \forall n \in \mathbf{N}, t \in \mathbf{T} \quad (21)$$

where $C_{g,t}^{gen}$ represents the generation cost of the g-th generator in the t-th time period; c_g is unit operational cost of generator; c_g^N is unit no-load cost of generator; c_g^S is unit startup cost of generator; $C_{w,t}^{wcur}$ represents the wind curtailment penalty cost of the w-th wind farm in the t-th time period; c_w is the penalty coefficient for wind curtailment of wind farm; $C_{n,t}^{shed}$ represents the load shedding penalty cost at node n in the t-th time period; c_l is the penalty coefficient for load shedding. Sum the above costs in the whole system and the modeling scope to obtain the operation cost C^{op} as follows:

$$C^{op} = \sum_{g \in \mathbf{G}, t \in \mathbf{T}} C_{g,t}^{gen} + \sum_{w \in \mathbf{W}, t \in \mathbf{T}} C_{w,t}^{wcur} + \sum_{n \in \mathbf{N}, t \in \mathbf{T}} C_{n,t}^{shed} \quad (22)$$

The construction cost at the planning stage includes equipment installation cost and power purchase cost. The total construction cost of HFC and HFGT are calculated as follows:

$$\begin{aligned} C^{pl} = c_f^{ins} \mid \mathbf{F} \mid + c_f^{pow} \sum_{f \in \mathbf{F}} P_f^{Frated} \\ + c_s^{ins} \mid \mathbf{S} \mid + c_s^{pow} \sum_{s \in \mathbf{S}} P_s^{Srated} \end{aligned} \quad (23)$$

where c_f^{ins} and c_s^{ins} are the unit installation cost of HFC and HFGT, respectively; c_f^{pow} and c_s^{pow} are the unit power purchase cost of HFC and HFGT, respectively.

3.2 Bi-level optimal configuration model

Based on the above cost analysis, the following optimal configuration model is formed.

$$\min \quad C^{op} \times DAY + C^{pl} \times CRF \quad (24)$$

$$\begin{aligned} s.t. \quad & Eq.(1) - (17) \\ & P^{Fmin} \leq P_f^{Frated} \leq P^{Fmax}, \forall f \in \mathbf{F} \\ & P^{Smin} \leq P_s^{Srated} \leq P^{Smax}, \forall s \in \mathbf{S} \end{aligned} \quad (25)$$

where P^{Fmin} and P^{Fmax} are minimum and maximum configurable hydrogen input power of HFC, respectively; P^{Smin} and P^{Smax} are minimum and maximum configurable hydrogen input power of HFGT, respectively; DAY stands for the number of days in a year; CRF stands for capital recovery factor and is defined as

$$CRF = \frac{\gamma(1+\gamma)^\alpha}{(1+\gamma)^\alpha - 1} \quad (26)$$

where γ is the appropriate discount rate and α is the economic lifetime of the project.

The optimal configuration model described above is a MILP problem mathematically, which is to optimize the cost based on the given configuration scheme. This optimal configuration model will participate in the evaluation of the optimal configuration scheme. Prior to the MILP, there should be an upper layer to generate the configuration scheme. The upper layer submits the generated configuration scheme to the lower MILP layer for cost evaluation, and then feeds back the results to the upper layer for improvement of the configuration scheme. Through the iteration of the upper and lower layers, the configuration scheme meeting the requirements is finally obtained.

4 Bi-level optimal configuration method

The obstacle in solving the two-level optimization model proposed in Section 3 are mainly concentrated in the upper layer. The accurate and efficient generation of configuration scheme in the upper layer is the basis of solution. An improved PSO algorithm is used for the upper layer of the proposed bi-level optimal configuration model. PSO is a population-based optimization technique. Each particle in the particle swarm has two attributes: velocity and position. The velocity represents the direction and distance the particle moves in the next iteration, and the position is a solution to the problem. Although the velocity and the position are multi-dimensional variables, they are independent of each other, so the velocity update equation of one dimension is described as follows:

$$\begin{aligned} V_{p,i+1} = \omega_i V_{p,i} + C_1 R_1 (PB_{p,i} - P_{p,i}) \\ + C_2 R_2 (GB_i - P_{p,i}) \end{aligned} \quad (27)$$

The position update equation of one dimension is described as follows:

$$P_{p,i+1} = P_{p,i} + V_{p,i} \quad (28)$$

where ω_i is the the inertia weight in the i-th iteration; $V_{p,i}$ is the velocity of the p-th particle in the i-th iteration; $P_{p,i}$ is the position of the p-th particle in the i-th iteration; C_1 and C_2 are the individual-cognition parameter and social learning parameter, respectively; R_1 and R_2 are both random values; $PB_{p,i}$ is individual best position of the p-th particle in the i-th iteration; GB_i is global best position in the i-th iteration.

In the proposed optimal configuration model, in order to achieve location and capacity at the same time, an array containing the capacity and location of HFC and HFGT will participate in the PSO iteration as the position of particle. However, this raises two problems. First, there is an order of magnitude difference between the capacities of HFC and HFGT. Using the same particle constraint will lead to large error or even non convergence of the optimization. Second, the dimension of particle position will be twice the number of nodes, and the high dimension will expand the search scope. It is necessary to improve the global optimization ability to avoid falling into local optimization, but it is also necessary to improve the local optimization ability at an appropriate time to ensure the convergence of the algorithm. The difference between HFC and HFGT in the order of magnitude of capacity can be handled by independently initializing and updating the particle position and velocity. The requirement of the algorithm for the optimization ability can be achieved by adjusting the inertia weight ω in the iteration. The inertia weight ω is utilized to balance the local exploitation and global exploration. The larger ω, the stronger the global optimization ability, but the weaker the local optimization ability. On the contrary, the weaker the global optimization ability, the stronger the local optimization ability. In this problem, the previous iteration needs strong global optimization ability, and in the later stage, it needs to carry out local optimization without changing the pattern of the solution to improve the convergence and stability of the solution. At this time, it is necessary to reduce the global optimization ability and improve the local optimization ability. Therefore, a nonlinear decreasing inertia weight is applied to the velocity iteration formula, which can maintain strong global optimization ability in a long period of time,

and improve the local optimization ability in the later period.

$$\omega_i = \omega_{max} - \left(\frac{iter}{iter_{max}}\right)^2 (\omega_{max} - \omega_{min}) \tag{29}$$

where ω_{max} and ω_{min} are the maximum and minimum inertia weight, respectively; $iter$ is the iteration order; $iter_{max}$ is maximum number of iterations.

The upper layer based on improved PSO is combined with the lower layer built by MILP to form a bi-level optimal configuration method. The solution flow of the method is given in Algorithm 1.

Algorithm 1: Bi-level optimization algorithm based on improved PSO

input : Maximum number of iterations $Iter_{max}$, Minimum number of iterations $Iter_{min}$, Error tolerance $ErrTol$.
output: Configuration array of fuel cell $FC = [fc_1, fc_2, \ldots, fc_N]$, Configuration array of gas turbine $GT = [gt_1, gt_2, \ldots, gt_N]$.

Construct $2N$ dimensional particle position array $PA \leftarrow [fc_1, fc_2, \ldots, fc_N, gt_1, gt_2, \ldots, gt_N]$;
Initialize particle swarm parameters;
for $i \leftarrow 1$ **to** $Iter_{max}$ **do**
  Update ω in Eq.(29);
  for $p \leftarrow 1$ **to** Pop **do**
    Calculate particle velocities $V[p,i]$ in Eq.(27);
    Calculate particle positions $P[p,i]$ in Eq.(28);
    $Obj[p,i] \leftarrow solve(\text{MILP}(P[p,i]))$;
    $Fit[p,i] \leftarrow Obj[p,i]$;
    Update $PB[p,i]$;
  end
  Update $GB[i]$;
  $FF[i] \leftarrow solve(\text{MILP}(GB[i]))$;
  if $i \geq Iter_{min}$ **then**
    if $FF[i - Iter_{min}] - FF[i] \leq ErrTol$ **then**
      $PA \leftarrow GB[i]$;
      break;
    end
  end
end
$FC \leftarrow PA[1:N]$;
$GT \leftarrow PA[N+1:2N]$.

After achieving the optimal solution, in order to analyze the marginal utility of system resources, the shadow price of optimal configuration can be obtained by dual method for analysis. However, considering that there is no duality in the MILP, it is necessary to fix the binary variables in the MILP with the optimal result first, so that it can be transformed into a linear programming problem, and then substitute FC and GT to get the shadow price.

5 Case study

5.1 Test case and implementation

The hybrid HtP system optimal configuration model is applied on a modified IEEE one area RTS-96 [32]. Based on the IEEE one area RTS-96, two wind farms are locateded at node 14 and node 22, respectively, to replace the traditional units in the original location. After removing the traditional units of these two nodes, the system still has 26 traditional units distributed on 9 nodes. The output of the wind farms is set to 80% of the total system load, resulting in a high renewable energy penetration according to Eq. 7. HPS stations are set up at the same nodes as the wind farms, with their rated power matching the output of the wind farm, which is 500MW and 1500MW, respectively. The efficiency of electro-hydrogen conversion of the electrolytic cell is set to 90%.

In order to reflect the contributions of hybrid HtP system on power system reliability in extreme situation, the maximum transmission capacity of transmission lines is set to 60% of the original system, and the load level is increased to 120%. Other unspecified power system parameters are imported from Matpower case file. The test case is shown in Fig. 2, in which HHP station is the schematic position.

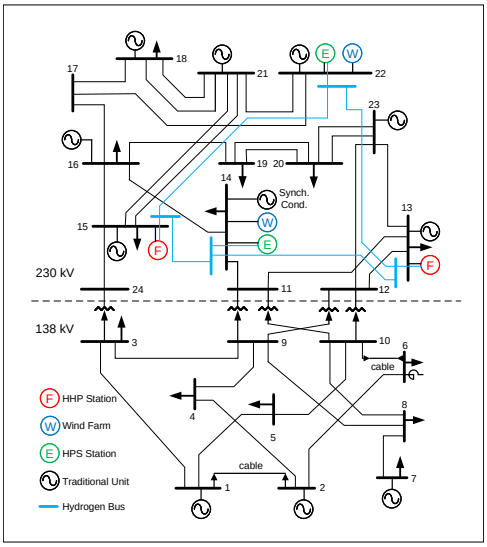

Fig. 2: Modified IEEE one area RTS-96

In addition to specific objective parameters, certain penalty coefficients have been established. The penalty coefficient for wind curtailment is designated as 20 CNY/MW, while the penalty coefficient for load shedding is set at 50 CNY/MW. Additionally, the installation cost and power purchase cost for HFC are 100,000 CNY/set and 400,000 CNY/MW, respectively, and the efficiency is 70%. The installation cost and power purchase cost for the HFGT are denoted as 200,000 CNY/set and 50,000 CNY/MW, respectively, with an efficiency of 50%. The anticipated service life of the project spans 20 years and the discount rate is 10%.

The program is encoded by Python and implemented on a desktop with a 6 core AMD Ryzen 5 3600 processor and 16 GB RAM. The MILP is solved by Gurobi 9.5.2 and the MIP gap is set at 0.01%. The parameters of the improved PSO are shown in Table 1.

Table 1 Parameters of the improved PSO

Parameter	Value	Parameter	Value
C_1	2	P^{Fmin}	100MW
C_2	2	P^{Fmax}	500MW
ω_{max}	1.5	P^{Smin}	500MW
ω_{min}	0.5	P^{Smax}	5000MW
$Iter_{min}$	8	$ErrTol$	0.0001
$Iter_{max}$	50	Pop	10

5.2 Simulation results

The optimization results of the proposed configuration model are presented in this subsection. The program converges to an optimal solution after 26 iterations and 270 seconds. The iteration of the solution is shown in Fig. 3.

The results of location and capacity of HFC and HFGT are presented in Table 2. HFC prefers distributed location and capacity, while HFGT is centralized. In addition, all HtP equipment are located in 138kV power grid, which has no renewable energy power generation. The hybrid HtP system indirectly shares the renewable

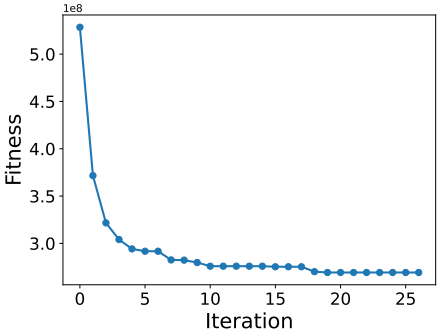

Fig. 3: The iteration of the solution

energy from the 220kV grid to the 138kV grid through hydrogen electricity conversion.

Table 2 Location and capacity of hybrid HtP system

HtP equipment	Location	Capacity[MW]
HFC	5	100
HFC	6	173
HFC	10	138
HFC	12	138
HFGT	8	831

Taking the HFC located at node 10 as an example, the hydrogen consumption source of HFC is shown in the Fig. 4. Under the combined hydrogen supply of the two HPS stations, the HFC maintains full load operation during the whole time period. Similar operating characteristics also occur on other HFCs and HFGT.

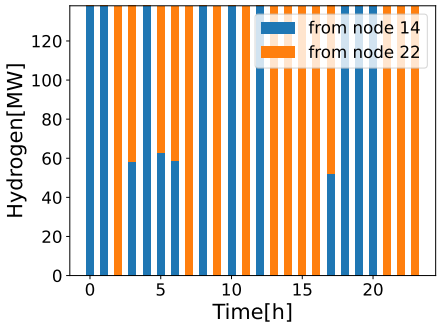

Fig. 4: The hydrogen consumption of HFC at node 10

Direct the attention to the HPS station. In the case setting, the hydrogen production capacity of the two HPS stations is different due to different renewable energy output levels. At the 14 node HPS station with weak hydrogen production capacity, its hydrogen production and consumption dynamics are shown in the Fig. 5. The hydrogen produced by HPS station is basically balanced with the supply to HHP station, and the hydrogen storage in the station is maintained at a low level. During the hours spanning from 10 o'clock to 17 o'clock, there is a reduction in renewable energy output and the hydrogen production capacity was insufficient. The demand for hydrogen allocated by the system from the HPS station decreases, resulting in a slight increase in hydrogen storage. These stored hydrogen supplies the hydrogen load after 17 o'clock. From the perspective of hydrogen flow direction, hydrogen mainly flows to HFCs, while a minor fraction of the hydrogen stream is directed towards the HFGT during peak hydrogen demand and periods of hydrogen surplus.

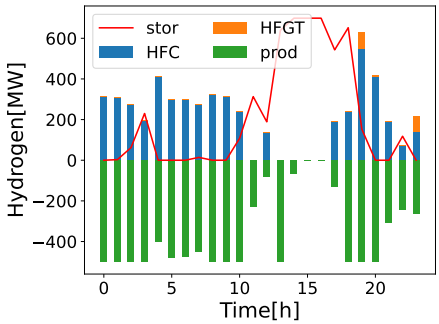

Fig. 5: The hydrogen production and consumption HPS station at node 14

The situation of 22 node HPS station is different. Due to the abundant renewable energy resources and strong hydrogen production capacity, before 8:00, the renewable energy output was large, and the HPS station produced hydrogen at the maximum hydrogen production rate, and the hydrogen storage in the station has been steadily and rapidly increasing. After 8 o'clock, the output of renewable energy weakened, and the hydrogen production also declined, making it difficult to cover the hydrogen load. A unified analysis of the hydrogen dynamics of the 14 node and 22 node HPS stations shows that most of the hydrogen load of the system at this time is borne by the 22 node HPS station. A large amount of hydrogen stored before 8 o'clock filled the shortage of hydrogen supply at this time. As for the direction of hydrogen, nearly half of the hydrogen in the 22 node HPS station is supplied to the hfgt in most time periods, except for the time period when all the hydrogen loads of the system are supplied. The hydrogen production and consumption dynamics are shown in the Fig. 6.

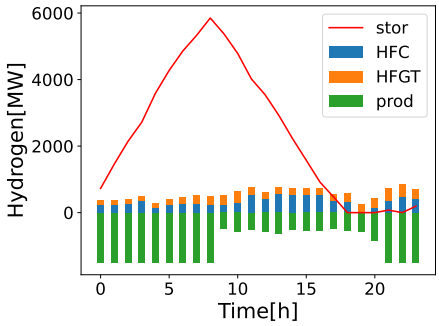

Fig. 6: The hydrogen production and consumption HPS station at node 22

The above shows the solutions and dynamics of the bi-level optimal configuration model. These results basically reflect the operation characteristics of the hybrid HTP system and meet the corresponding expectations. Based on these results, the influence of hybrid HtP system on the whole power system will be further discussed.

5.3 Discussions

First, the output of traditional units is analyzed. The output of 26 traditional generators in the power system is shown in Fig. 7. Among the 26 generators, 15 do not startup in the whole dispatching cycle, 4 startup and shutdown more than once in operation, and the rest basically maintained stable output. Generator startup and no-load will bring additional operating costs, which is reflected in the objectives of the operation optimization model. The hybrid HtP system and the entire hydrogen system are coupled with the power system, which plays the role of energy storage. By converting the surplus power

energy into hydrogen energy, the long-term storage of power is realized, which provide abundant and flexible dispatching resources for the power system. These dispatching resources share the operating pressure of traditional units, resulting a lower operation cost.

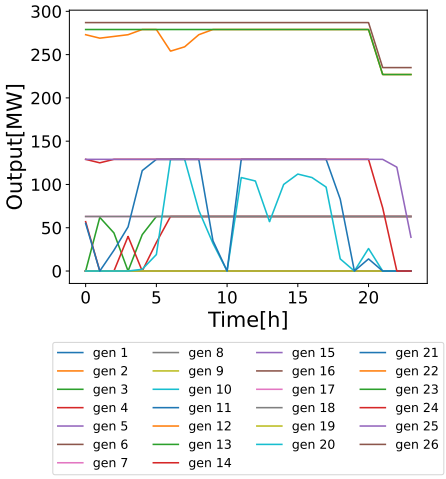

Fig. 7: The output of traditional units

Second, as the energy storage of the power system, the hybrid HtP system has also made outstanding contributions to strengthening the accommodation of renewable energy and improving the utilization level. In this case, although the penetration of renewable energy has reached 80%, on the one hand, the wind power output shows great fluctuation, on the other hand, the distribution of wind power is concentrated and marginalized, so the utilization of renewable energy has great challenges. The wind power accommodation of the power system without hybrid HtP system is shown in the Fig. 8.

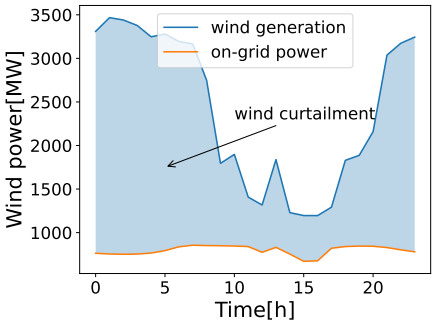

Fig. 8: Total wind curtailment of power system without hybrid HtP system

The output of wind power is large at night and small during the day, which makes the wind curtailment concentrated at night. By analyzing the dynamics of the HPS stations, it can be found that the electrolytic cell is consuming this part of power at its maximum operating power at this time, and the surplus wind power is also quickly fixed in the hydrogen storage tanks of the HPS stations in this way. The wind power accommodation of the power system with hybrid HtP system is shown in the Fig. 9. This energy transfer across time and space indirectly suppresses the fluctuation of wind power output, and provides guarantee for the efficient and stable operation of high penetration renewable energy power system.

Third, the hybrid HtP system plays an important role in improving the power supply reliability of power system. In this case, the transmission conditions and load demand of the power system are set strictly. Fig. 10 shows the load shedding of the system when the

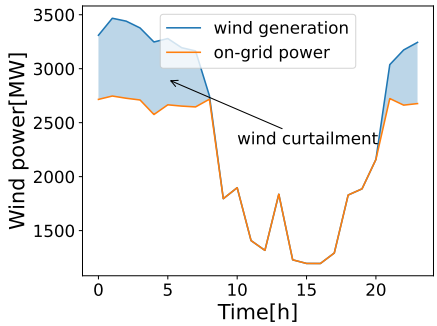

Fig. 9: Total wind curtailment of power system with hybrid HtP system

hybrid HtP system is not configured. The load supply of the system is only 79.16%. However, with the support of the hybrid HtP system, the load shedding performance of the system is good, as shown in Fig. 11. The load supply can basically track the load demand curve, and the load supply of the system reaches 97.40%. The existing load loss is mainly caused by the power shortage of node 7, 8 and 9.

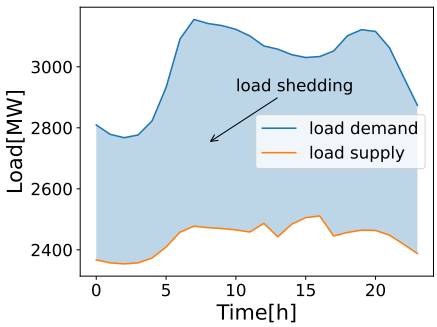

Fig. 10: Total load shedding of power system without hybrid HtP system

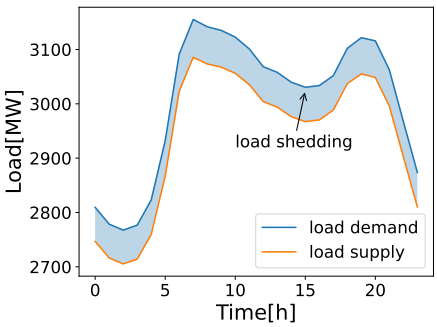

Fig. 11: Total load shedding of power system supported by hybrid HtP system

Finally, the marginal utility of system resources is analyzed using the shadow price. For HPS station, its hydrogen storage capacity has been maximized, and there is still some room for development of hydrogen production capacity. For HHP stations, HFC is also used to the greatest extent, but the shadow price of HFGT is 0. For traditional generating units, the shadow price of maximum and minimum generating power is positive, but the shadow price of spinning reserve is basically 0. From the analysis of shadow price, it can be seen that

hybrid HtP system plays an important role in low-cost and efficient operation of power system, but this case still expects greater power storage and transfer capacity, and hybrid HtP system has greater potential in large-scale power system.

6 Conclusion

In this paper, the hybrid HtP system is proposed as a scheme to improve the performance of the hydrogen to electricity. The hybrid HtP system is composed of HFC and HFGT to achieve complementary output power. However, the hybrid HtP system is coupled with hydrogen production and storage system, as well as power system. The characteristics of each subsystem and coupling characteristics are complex. In addition, the multiple support potential of hybrid HtP system for power system still needs to be fully explored. This paper first constructs a high penetration renewable energy power system considering hybrid HtP system, including traditional generating units, renewable energy power generation system, hybrid HTP system and power grid. These power system subsystems and their energy coupling are modeled separately. Secondly, based on the above power system models, a bi-level hybrid HtP system optimal configuration model including planning and operation is constructed, and the optimal configuration scheme is obtained through the iteration between the upper and lower layers. In order to solve this problem, a bi-level optimal configuration method based on improved PSO algorithm is proposed, which solves the problem of insufficient algorithm performance in the optimization process. Finally, the bi-level optimal configuration model and its solution method are applied to IEEE one area RTS-96, and the solutions and operation dynamics of the model are obtained. Based on the optimization results, the further discussion falls on the contributions of hybrid HtP system to power system. The results show that the hybrid HtP system has a significant effect on optimizing the output cost of traditional units, improving the utilization of renewable energy, and reducing load shedding losses. In addition, through the analysis of the shadow price, it is concluded that the hybrid HtP system will make a greater contribution to the larger power system.

Based on this paper, further research is on-going to understand how much more benefits the hybrid HtP system will bring in a wider power output range. The impact of topology and energy interaction between HPS stations and HHP stations on planning and operation also needs to be further considered.

Nomenclature

Constants

α	The economic lifetime of the project (year)
Δt	Length of each period
η_e	Efficiency of electrolytic hydrogen production (%)
η_f	Efficiency of HFC generation (%)
η_s	Efficiency of HFGT generation (%)
γ	The discount rate (%)
c_f^{ins}	Unit installation cost of HFC (CNY/set)
c_f^{pow}	Unit power purchase cost of HFC (CNY/MW)
c_g	Unit operational cost of generator (CNY/MW)
c_g^N	unit no-load cost of generator (CNY/time)
c_g^S	Unit startup cost of generator (CNY/time)
c_l	Penalty coefficient for load shedding (CNY/MW)
c_s^{ins}	Unit installation cost of HFGT (CNY/set)
c_s^{pow}	Unit power purchase cost of HFGT (CNY/MW)
c_w	Penalty coefficient for wind curtailment (CNY/MW)
CRF	Capital recovery factor
DAY	Average annual number of days
P^{Fmax}	Maximum configurable hydrogen input power of HFC (MW)
P^{Fmin}	Minimum configurable hydrogen input power of HFC (MW)
P^{Smax}	Maximum configurable hydrogen input power of HFGT (MW)
P^{Smin}	Minimum configurable hydrogen input power of HFGT (MW)
P^{Tmax}	Maximum transmission capacity of hydrogen blended natural gas pipeline
P_b^{max}	Maximum transmission power of branch
REP	Renewable energy penetration (%)
x_b	Branch impedance

Indices

b	Index of branches in power system, running from 1 to B
e	Index of HPS stations, running from 1 to E
f	Index of HFCs, running from 1 to F
g	Index of generators, running from 1 to G
n	Index of nodes in power system, running from 1 to N
s	Index of HFGTs, running from 1 to S
t	Index of time periods, running from 1 to T
w	Index of wind farms, running from 1 to W

Sets

B	Set of branches in power system
E	Set of HPS stations
F	Set of HFCs
G	Set of traditional generators
N	Set of nodes in power system
S	Set of HFGTs
T	Set of time periods
W	Set of wind farms

Variables

$\delta_{n,t}$	Voltage phase (rad)
$\theta_{b,t}$	Phase difference of voltages (rad)
C^{op}	Operation cost of the system (CNY)
C^{pl}	Construction cost of the system (CNY)
$C_{g,t}^{gen}$	Generation cost of the traditional units (CNY)
$C_{n,t}^{shed}$	load shedding penalty cost (CNY)
$C_{w,t}^{wcur}$	wind curtailment penalty cost (CNY)
$E_{e,t}$	Capacity of hydrogen stored at HPS station (MWh)
$E_{e,t}^{rated}$	Rated capacity of hydrogen stored at HPS station (MWh)
$P_{b,t}$	Active power flowing on the branch (MW)
$P_{e,t}^{Erated}$	Rated input hydrogen power of electrolytic cell (MW)
$P_{e,t}^{E}$	Input hydrogen power of electrolytic cell (MW)
$P_{f,e,t}^{F}$	Input hydrogen power of HFC (MW)
P_{f}^{Frated}	Rated input hydrogen power of HFC (MW)
$P_{g,t}^{G}$	The output of generator (MW)
$P_{g,t}^{Gmax}$	Maximal output of generator (MW)
$P_{g,t}^{Gmin}$	Minimal output of generator (MW)
$P_{g,t}^{R}$	Spinning reserve of generator (MW)
$P_{n,t}^{L}$	Load (MW)
$P_{n,t}^{LS}$	Load shedding (MW)
$P_{s,e,t}^{S}$	Input hydrogen power of HFGT (MW)
P_{s}^{Srated}	Rated input hydrogen power of HFGT (MW)
$P_{w,t}$	Wind power output of wind farm (MW)
$P_{w,t}^{WC}$	Wind curtailment of wind farm (MW)
R_g	Maximum ramp rate of generator (MW/h)
R_g^{10}	Outage ramping limit in 10 minutes of generator (MW)
$u_{g,t}$	Commitment status of generator (binary)
$v_{g,t}$	Startup status of the generator (binary)

Acknowledgment

This work is supported by the National Natural Science Foundation of China (52177112).

7 References

1 Yue, M., Lambert, H., Pahon, E., Roche, R., Jemei, S., Hissel, D.: 'Hydrogen energy systems: A critical review of technologies, applications, trends and challenges', *Renewable and Sustainable Energy Reviews*, 2021, **146**, pp. 111180

2 Arsad, A.Z., Hannan, M.A., Al.Shetwi, A.Q., Mansur, M., Muttaqi, K.M., Dong, Z.Y., et al.: 'Hydrogen energy storage integrated hybrid renewable energy systems: A review analysis for future research directions', *International Journal of*

Hydrogen Energy, 2022, **47**, (39), pp. 17285–17312
3 Li, H., Qin, B., Jiang, Y., Zhao, Y., Shi, W.: 'Data-driven optimal scheduling for underground space based integrated hydrogen energy system', *IET Renewable Power Generation*, 2022, **16**, (12), pp. 2521–2531
4 Gao, R., Zhang, Q., Zhao, Y., Han, Z., Sun, C., Sheng, J., et al.: 'Regulating Polysulfide Redox Kinetics on a Self-Healing Electrode for High-Performance Flexible Lithium-Sulfur Batteries', *Advanced Functional Materials*, 2022, **32**, (15), pp. 2110313
5 Scolaro, M., Kittner, N.: 'Optimizing hybrid offshore wind farms for cost-competitive hydrogen production in Germany', *International Journal of Hydrogen Energy*, 2022, **47**, (10), pp. 6478–6493
6 Maghami, M.R., Hassani, R., Gomes, C., Hizam, H., Othman, M.L., Behmanesh, M.: 'Hybrid energy management with respect to a hydrogen energy system and demand response', *International Journal of Hydrogen Energy*, 2020, **45**, (3), pp. 1499–1509
7 Zhang, Z., Qin, B., Gao, X., Ding, T.: 'Cnn-lstm based power grid voltage stability emergency control coordination strategy', *IET Generation, Transmission & Distribution*, 2023, **17**, (16), pp. 3559–3570
8 Alirahmi, S.M., Assareh, E., Chitsaz, A., Ghazanfari.Holagh, S., Jalilinasrabady, S.: 'Electrolyzer-fuel cell combination for grid peak load management in a geothermal power plant: Power to hydrogen and hydrogen to power conversion', *International Journal of Hydrogen Energy*, 2021, **46**, (50), pp. 25650–25665
9 Genovese, M., Schlüter, A., Scionti, E., Piraino, F., Corigliano, O., Fragiacomo, P.: 'Power-to-hydrogen and hydrogen-to-X energy systems for the industry of the future in Europe', *International Journal of Hydrogen Energy*, 2023, **48**, (44), pp. 16545–16568
10 Zhang, Y., Wang, L., Wang, N., Duan, L., Zong, Y., You, S., et al.: 'Balancing wind-power fluctuation via onsite storage under uncertainty: Power-to-hydrogen-to-power versus lithium battery', *Renewable and Sustainable Energy Reviews*, 2019, **116**, pp. 109465
11 Tarasenko, A.B., Kiseleva, S.V., Popel, O.S.: 'Hydrogen energy pilot introduction – Technology competition', *International Journal of Hydrogen Energy*, 2022, **47**, (23), pp. 11991–11997
12 Ferraren.De.Cagalitan, D.D.T., Abundo, M.L.S.: 'A review of biohydrogen production technology for application towards hydrogen fuel cells', *Renewable and Sustainable Energy Reviews*, 2021, **151**, pp. 111413
13 Cheng, C., Cherian, J., Sial, M.S., Zaman, U., Niroumandi, H.: 'Performance assessment of a novel biomass-based solid oxide fuel cell power generation cycle; Economic analysis and optimization', *Energy*, 2021, **224**, pp. 120134
14 Singla, M.K., Nijhawan, P., Oberoi, A.S.: 'Hydrogen fuel and fuel cell technology for cleaner future: a review', *Environ Sci Pollut Res*, 2021, **28**, (13), pp. 15607–15626
15 Olabi, A.G., Wilberforce, T., Abdelkareem, M.A.: 'Fuel cell application in the automotive industry and future perspective', *Energy*, 2021, **214**, pp. 118955
16 Alhuyi.Nazari, M., Fahim.Alavi, M., Salem, M., Assad, M.E.H.: 'Utilization of hydrogen in gas turbines: a comprehensive review', *International Journal of Low-Carbon Technologies*, 2022, **17**, pp. 513–519
17 Serbin, S., Burunsuz, K., Chen, D., Kowalski, J.: 'Investigation of the characteristics of a low-emission gas turbine combustion chamber operating on a mixture of natural gas and hydrogen', *Polish Maritime Research*, 2022, **nr 2**, pp. 64–76
18 Öberg, S., Odenberger, M., Johnsson, F.: 'The value of flexible fuel mixing in hydrogen-fueled gas turbines – A techno-economic study', *International Journal of Hydrogen Energy*, 2022, **47**, (74), pp. 31684–31702
19 Meng, X., Chen, M., Gu, A., Wu, X., Liu, B., Zhou, J., et al.: 'China's hydrogen development strategy in the context of double carbon targets', *Natural Gas Industry B*, 2022, **9**, (6), pp. 521–547
20 Rocha, R.C., Costa, M., Bai, X.S.: 'Combustion and Emission Characteristics of Ammonia under Conditions Relevant to Modern Gas Turbines', *Combustion Science and Technology*, 2021, **193**, (14), pp. 2514–2533
21 Wang, Z., Jia, Y., Cai, C., Chen, Y., Li, N., Yang, M., et al.: 'Study on the Optimal Configuration of a Wind-Solar-Battery-Fuel Cell System Based on a Regional Power Supply', *IEEE Access*, 2021, **9**, pp. 47056–47068. conference Name: IEEE Access
22 Gupta, J., Nijhawan, P., Ganguli, S.: 'Optimal sizing of different configuration of photovoltaic, fuel cell, and biomass-based hybrid energy system', *Environ Sci Pollut Res*, 2022, **29**, (12), pp. 17425–17440
23 Zhou, J., Wu, Y., Zhong, Z., Xu, C., Ke, Y., Gao, J.: 'Modeling and configuration optimization of the natural gas-wind-photovoltaic-hydrogen integrated energy system: A novel deviation satisfaction strategy', *Energy Conversion and Management*, 2021, **243**, pp. 114340
24 Wang, Q., Duan, L., Lu, Z., Zheng, N.: 'Thermodynamic and economic analysis of a multi-energy complementary distributed cchp system coupled with solar thermochemistry and active energy storage regulation process', *Energy Conversion and Management*, 2023, **292**, pp. 117429
25 Ding, X., Sun, W., Harrison, G.P., Lv, X., Weng, Y.: 'Multi-objective optimization for an integrated renewable, power-to-gas and solid oxide fuel cell/gas turbine hybrid system in microgrid', *Energy*, 2020, **213**, pp. 118804
26 Guo, Y., Yu, Z., Li, G., Zhao, H.: 'Performance assessment and optimization of an integrated solid oxide fuel cell-gas turbine cogeneration system', *International Journal of Hydrogen Energy*, 2020, **45**, (35), pp. 17702–17716
27 Safari, S., Hajilounezhad, T., Ehyaei, M.A.: 'Multi-objective optimization of solid oxide fuel cell/gas turbine combined heat and power system: A comparison between particle swarm and genetic algorithms', *International Journal of Energy Research*, 2020, **44**, (11), pp. 9001–9020
28 Abdou, I., Tkiouat, M.: 'Unit Commitment Problem in Electrical Power System: A Literature Review', *IJECE*, 2018, **8**, (3), pp. 1357–1372
29 Cerniauskas, S., Jose.Chavez.Junco, A., Grube, T., Robinius, M., Stolten, D.: 'Options of natural gas pipeline reassignment for hydrogen: Cost assessment for a Germany case study', *International Journal of Hydrogen Energy*, 2020, **45**, (21), pp. 12095–12107
30 Chae, M.J., Kim, J.H., Moon, B., Park, S., Lee, Y.S.: 'The present condition and outlook for hydrogen-natural gas blending technology', *Korean J Chem Eng*, 2022, **39**, (2), pp. 251–262
31 Nayebossadri, S., Speight, J.D., Book, D.: 'Hydrogen separation from blended natural gas and hydrogen by Pd-based membranes', *International Journal of Hydrogen Energy*, 2019, **44**, (55), pp. 29092–29099
32 Grigg, C., Wong, P., Albrecht, P., Allan, R., Bhavaraju, M., Billinton, R., et al.: 'The IEEE Reliability Test System-1996. A report prepared by the Reliability Test System Task Force of the Application of Probability Methods Subcommittee', *IEEE Transactions on Power Systems*, 1999, **14**, (3), pp. 1010–1020